TECHNICAL MEMORANDUM

X-442

TRANSONIC FLUTTER INVESTIGATION OF MODELS OF PROPOSED

HORIZONTAL TAILS FOR THE X-15 AIRPLANE

By Lou S. Young

Langley Research Center
Langley Field, Va.

Declassified by authority of NASA
Classification Change Notices No. _67_
Dated ** _6/29/66_

DECLASSIFIED- AUTHORITY
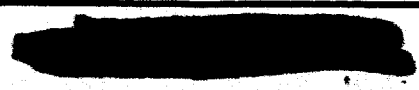US: 1286   DROBKA TO LEBOW
             MEMO DATED
             6/8/66

NATIONAL AERONAUTICS AND SPACE ADMINISTRATION

WASHINGTON   February 1961

TECHNICAL MEMORANDUM X-442

TRANSONIC FLUTTER INVESTIGATION OF MODELS OF PROPOSED

HORIZONTAL TAILS FOR THE X-15 AIRPLANE*

By Lou S. Young

33328

SUMMARY

A flutter investigation at Mach numbers between 0.79 and 1.47 has been made in the Langley transonic blowdown tunnel of dynamically and elastically scaled models of the original design and of a revised design for the all-movable horizontal tail of the X-15 airplane. A third design, which was not tested in the present investigation, was finally used in the airplane. The two designs investigated herein differed only in panel mass and stiffness distributions. Both designs had a planform which was swept back and tapered, and in each case the tail panels were independently mounted and actuated. The semispan models were mounted in a sting fuselage so that the airplane stiffnesses at the panel root were simulated, with provision for changing the stiffness in pitch. The airplane-fuselage degrees of freedom were not simulated.

One model of the original design simulated the panel stiffness distributions which were calculated for the airplane at standard sea-level temperature conditions. Other models of both the original and the revised designs simulated the calculated airplane panel stiffness distributions for a reduced skin stiffness caused by transient aerodynamic heating.

The standard-temperature model of the original design had an adequate flutter safety margin over the Mach number range of the tests (that is, the model was flutter free at dynamic pressures up to 32 percent higher than those for simulated sea-level conditions). The high-temperature models of both the original and the revised designs had adequate flutter safety margins at Mach numbers up to about 1.1 but had inadequate safety margins at high Mach numbers. An increase in pitching stiffness for a high-temperature model of the original design to 118 percent of the scaled airplane value gave a configuration which had an adequate safety margin throughout the Mach number range of the investigation.

*Title, Unclassified.

INTRODUCTION

A program for determining the flutter characteristics of the components of the X-15 airplane has been undertaken by the Langley Research Center. Included in this program have been investigations at supersonic and hypersonic speeds (refs. 1 and 2, respectively) of dynamically and elastically scaled models of the original design for the airplane all-movable horizontal tail. The present paper describes an investigation made at Mach numbers between 0.79 and 1.47 in the Langley transonic blowdown tunnel of dynamically and elastically scaled models of the original and of a revised design for the airplane horizontal tail.

The original and revised designs had the same planform and each tail panel was independently mounted and actuated. Both designs had the same pitching stiffness at the panel root; however, the revised design had lower bending stiffness near the tip, higher bending stiffness at inboard stations, and was somewhat heavier than the original design. A third design, which was not tested in the present investigation, was finally used in the airplane.

One model of the original design simulated the panel stiffness distributions which were calculated for the airplane at standard sea-level temperature conditions. Other models of both the original and revised designs simulated the calculated airplane stiffness distributions for a reduced skin stiffness resulting from transient aerodynamic heating (ref. 3). The transient heating effects were calculated by the aircraft manufacturer for that part of the airplane flight path which gave the greatest stiffness reduction. This condition occurs during descent at a very high Mach number and altitude. Later in the descent, as the Mach number approaches transonic values, the stiffnesses would tend to increase so that the present models may yield conservative results.

Semispan models were used in the investigation, and the models were flexibly mounted in a sting fuselage so as to simulate the pitch, roll, and yaw freedoms at the intersection of the pitch axis and panel root. Tests were also made with higher levels of pitching stiffness at the panel root. The airplane-fuselage degrees of freedom were not simulated.

SYMBOLS

b local streamwise semichord, ft

b_a average streamwise semichord of exposed panel, ft
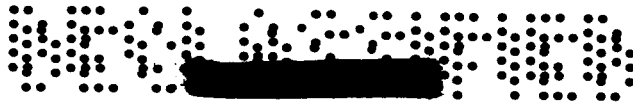
b_s average streamwise semichord of streamwise strip, ft

EI bending stiffness, lb-ft^2

f_f flutter frequency, cps

GJ torsional stiffness, lb-ft^2

g structural damping coefficient of first natural vibration mode

I_s moment of inertia of streamwise strip about lateral axis through strip center of gravity, slug-ft^2

I_θ moment of inertia of panel (including spindle) in pitch about panel center of gravity, slug-ft^2

I_ϕ moment of inertia of panel (including spindle) in roll about panel center of gravity, slug-ft^2

I_ψ moment of inertia of panel (including spindle) in yaw about panel center of gravity, slug-ft^2

k_θ simulated pitch stiffness at intersection of pitch axis and panel root, ft-lb/radian

k_ϕ simulated roll stiffness at intersection of pitch axis and panel root, ft-lb/radian

k_ψ simulated yaw stiffness at intersection of pitch axis and panel root, ft-lb/radian

l length scale factor, $\dfrac{\text{Typical model length}}{\text{Corresponding airplane length}}$

M Mach number

m mass scale factor, $\dfrac{\text{Typical model mass}}{\text{Corresponding airplane mass}}$

m' mass of panel (including spindle), slugs

m_s mass of streamwise strip, slugs

q dynamic pressure, lb/sq ft

s   span of panel, ft

T   static temperature, $^\circ R$

t   time scale factor,
$$\frac{\text{Time for tunnel airstream to move 1 model tail chord length}}{\text{Time for airplane to move 1 airplane tail chord length}}$$

V   velocity, fps

$\overline{V}$ reduced velocity based on a representative natural frequency,
$$\frac{V}{b_a \omega_i}$$

v   volume of frustrum of cone enclosing the tail panel, $\pi \int_0^s b^2 dy$, cu ft

X,Y,Z   longitudinal, lateral, and vertical axes, respectively

x_{cg} center-of-gravity location of streamwise strip, percent local streamwise chord measured from leading edge

y_{cg} center-of-gravity location of streamwise strip, percent of span measured from panel root

δ_s width of streamwise strip, ft

η nondimensional distance along reference axis,
$$\frac{\text{Distance from panel root along reference axis}}{\text{Length of exposed panel reference axis}}$$

μ mass ratio, $m'/\rho v$

ρ static air density, slugs/cu ft

ω_f flutter frequency, $2\pi f_f$, radians/sec

ω_i natural frequency of ith mode, radians/sec

Subscripts:

A   airplane

M   model

MODELS

Configurations

The model components, which were supplied by the aircraft manufacturer, consisted of five tail panels and the mount. Seven model configurations were investigated and are designated as follows: CO-96, HO-95, HO-99, HO-105, HO-137, HO-118, and HR-101. The code for these designations is as follows: "C" (for cold) indicates that the panel stiffnesses simulated the calculated airplane values at standard sea-level temperature, "H" (for hot) indicates that the panel stiffnesses simulated the calculated airplane values as affected by aerodynamic heating, "O" indicates the original design, "R" indicates the revised design, and the number following the dash gives the root pitch stiffness in percent of the scaled airplane value. Model HO-105 was not tested but was used to obtain flexibility influence coefficients.

Geometry

The semispan models were 1/12-size versions of the proposed horizontal tail panels for the airplane. A sketch of the models giving basic dimensions is shown in figure 1, where the dimensions given were the same for all the models to within ±0.07 inch.

The models had a planform incorporating 45° sweepback of the quarter-chord line, a panel aspect ratio of 1.24, and a panel taper ratio of 0.3. The model had a 66A005 airfoil section (manufacturer's designation), modified so that it had a 1 percent thickness at the trailing edge with a straight-line fairing between the trailing edge and 67 percent chord (point of tangency). Near the tip, the airfoil was further modified by increasing the thickness forward of the 15 percent chord. Airfoil ordinates are presented in figure 1, and some model geometric properties are listed in table I.

Scaling

In scaling the airplane properties it was required that the nondimensional mass and stiffness distributions should be the same for the model as for the airplane. The mass and stiffness levels for the model were obtained by specifying the scale factors for the fundamental quantities involved: length, mass, and time.

The size of the models was limited by tunnel-wall interference considerations, and on the basis of previous experience, the length scale factor was chosen to be
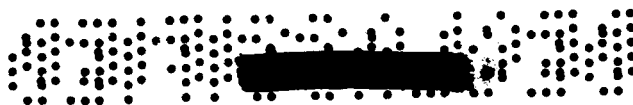
$$l = \frac{1}{12} \tag{1}$$

The mass scale factor was obtained from the requirement that the mass ratio μ be the same for both model and airplane. This gave

$$m = \frac{\rho_M}{\rho_A} l^3 \tag{2}$$

The density ratio was chosen to be $\rho_M / \rho_A = 1.275$.

The time scale factor was derived from the requirement that the reduced velocity $\overline{V}$ should be the same for the model as for the airplane. This gives

$$t = \left(\frac{V_M}{V_A}\right)^{-1} l$$

Since the Mach number is the same for both model and airplane,

$$t = \left(\frac{T_M}{T_A}\right)^{-1/2} l \tag{3}$$

The static temperature for the airplane T_A is a function only of altitude, and for sea-level altitude T_A was taken to be 519° R. However, during a tunnel run, the temperature drops continually as air is expended from the reservoir. A study of flutter data obtained previously indicated that 408° R was near the average value of T_M that could be expected during the present tests. These values of T_M and T_A were used in equation (3); hence, 0.786 was used as the value of T_M/T_A. The pertinent model and flow parameters and the design scale factors which apply to them are listed in table II.

The dynamic pressure and Mach number are quantities which are controllable during a run, whereas the temperature is not. If the dynamic pressure and Mach number are considered to be fixed, and a static temperature different from the design value is obtained, both the density and the velocity will be different from the values considered in the scaling. The density and velocity changes result, respectively, in values of mass

ratio and reduced velocity different from the design values. However, a combination of reduced velocity and mass ratio, which can be expressed in terms of the dynamic pressure

$$\frac{\overline{V}_M^2}{\mu_M} \propto q_M .$$

is independent of the temperature. This parameter is simulated exactly in the tests because the simulated altitude is interpreted in terms of the dynamic pressure. Thus, the scale factor in table II for dynamic pressure is used to convert the dynamic pressure for the airplane at any Mach number and altitude to the dynamic pressure for the model at the same Mach number and altitude. The dynamic pressure for the airplane is assumed to be that of the ICAO standard atmosphere (ref. 4). Note that for a given altitude q/M^2 has a constant value.

The effect of not individually satisfying exactly the mass ratio and reduced velocity is believed to be negligible in the present investigation. Experience with a wide variety of flutter models has indicated that, at a given Mach number, flutter tends to occur at a constant value of dynamic pressure regardless of the individual values of density and velocity, at least within the operational limits of the tunnel.

Panel Construction and Mounting

All panels had aluminum box spar and rib construction as seen in figure 2, which shows X-ray photographs of two of the tail panels. A photograph of a flutter-damaged panel which has had portions of the exterior cut away to expose the internal structure is presented in figure 3. (Paint was applied at intervals along the leading edges of the models as shown in fig. 3 to aid in observing the motion of the models during testing.) The tapered spar was fabricated from two hollow rectangular-cross-section pieces welded together. Aluminum-alloy caps which covered about one-fifth of the spar width were welded to the outside of the spar at top and bottom and extended from the root to about 40 percent of the panel span. A solid aluminum-alloy spindle having rectangular cross sections was welded inside the spar at the root and extended inboard of the root. The spindle (fig. 1) for model HR-101 was somewhat heavier than that for the other models. Aluminum-alloy root and tip ribs were of rectangular cross sections and were welded to the spar. Additional ribs having channel cross sections were also welded to the spar with the open sides facing outboard. Leading and trailing edges were made of pine, and balsa wood was used to fill voids in the airfoil shape. Small lead weights were glued into the structure at various
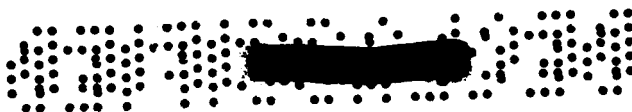
points to achieve the proper mass distribution. The entire outer surface of the panel was covered with lacquered silk.

The mounting system, shown in figure 4, allowed flexibility in the pitch, roll, and yaw degrees of freedom. The tail panel was fastened to two vertical tongues extending from the steel base spring mount (fig. 4) by means of two screws through the spindle. A steel stud threaded into one of the tongues was fastened at its other end to a steel cantilever beam, which was secured at its fixed end to a steel mounting block. Both the base spring mount and the beam mounting block were fastened securely to the fuselage mounting block, which was machined from solid aluminum alloy so that it faired into the 3-inch-diameter tunnel sting fuselage. The arrangement was such that the installation of cantilever beams having different bending stiffnesses would have a major effect on the root pitching stiffness only. Provision was made for the use of a locking bar between the cantilever beam and the fuselage mounting block to increase further the root pitching stiffness.

<div align="right">L
3
0
9</div>

Physical Properties

Natural vibration modes.- The natural vibration frequencies and node lines were found by exciting the models with an electromagnetic shaker. Salt crystals sprinkled on the panel during resonant vibrations depicted the node lines. The results obtained for the various configurations investigated are presented in figure 5. The frequencies are also listed in table III where the predominant characteristic of each vibration mode is indicated. In addition to the noted predominant characteristics, pitching motion of the panel was also evident in the first, third, and fourth modes.

The average values of the structural damping coefficient in the first natural vibration mode, as determined for each model from records of the decay of oscillations induced by plucking the model in still air, are presented in table III.

Stiffnesses.- The roll, pitch, and yaw stiffnesses at the intersection of the pitch axis with the panel root were measured by means of an optical system employing a cathetometer. The results are presented in table III. The rolling stiffness was measured only for model HR-101. The rolling stiffnesses for the other models, which were all of the original design, were probably somewhat lower than for model HR-101 because of their more flexible spindles (fig. 1).

The bending and torsion stiffness distributions along the span were also measured for each panel by means of an optical system which is described in reference 5. The reference axis used for these measurements

was approximately the 53-percent-chord line. The stiffness distributions which were obtained are presented in figure 6.

Flexibility influence coefficients, which were measured on model HO-105, are presented in table IV(a). These coefficients are the results of the following measurements: (1) translation deflections at 12 stations on the panel (fig. 7) due to loads applied at these stations, (2) translational deflections on the panel due to pitching and rolling moments applied at the root, and (3) pitch, roll, and yaw angular deflections at the intersection of the pitch axis and panel root due to loads applied to the panel stations and due to pitching, rolling, and yawing moments applied at the root. The system employed to measure the influence coefficients is described in the appendix.

The measured flexibility influence coefficients given in table IV(a) were averaged across the diagonal of the matrix to obtain the symmetrical matrix which is presented in table IV(b).

Mass properties.- The mass of each panel is presented in table III. The center-of-gravity location for one panel of the original design is shown in figure 1; the center-of-gravity locations for the other panels of the original design are believed to be at approximately the same location. The center-of-gravity location for the revised design panel is also presented in figure 1. The moments of inertia in roll, pitch, and yaw which were measured for some of the panels by means of a bifilar pendulum are given in table III. All masses, moments of inertia, and center-of-gravity locations given in table III and figure 1 were measured with the spindle attached to the panel.

Mass distribution data for a panel of the original design and for a panel of the revised design are presented in tables V(a) and V(b), respectively. The values for the original design were obtained by sawing the panel of model HO-99 (which was repaired after flutter testing) into streamwise strips as shown in the sketch in table V(a). These data have been corrected for the mass lost in sawing. Most of the data in table V(b) for the revised design were supplied by the model manufacturer and were obtained by sawing a panel similar to that of model HR-101 into strips normal to the 56.78-percent-chord line as shown in table V(b). However, the properties of the strip numbered "1" and of the spindle were measured on model HR-101 after flutter testing. The total mass of this composite model given in table V(b) is about 9 percent lower than that measured for model HR-101 as given in table III.

APPARATUS AND TESTS

The flutter tests were made in the Langley transonic blowdown tunnel which has a slotted test section. The test section is octagonal in cross section and measures $26\frac{1}{4}$ inches between sides. During operation of the tunnel, a preselected Mach number is set by means of a variable orifice downstream of the test section, and this Mach number is held approximately constant after the orifice is choked while the stagnation pressure, and thus the density, is increased. The static-density range is approximately 0.001 to 0.012 slug per cubic foot, and Mach numbers may be obtained with semispan models from subsonic values to a maximum value of about 1.45. It should be noted that, because of the expansion of the air in the reservoir during a run, the stagnation temperature continually decreases, and thus the test-section velocity is not uniquely defined by the Mach number. Additional details of the tunnel are contained in reference 6. Excellent agreement between flutter data obtained in the tunnel and in free air has been observed (ref. 7).

In the present flutter tests, the fuselage mounting block shown in figure 4 was fitted into a sting in such a way that the mounting block and sting formed a 3-inch-diameter fuselage which extended upstream into the subsonic flow region of the tunnel. This arrangement prevented the formation of shock waves off the fuselage nose which might reflect from the tunnel walls onto the model. The sting and model weighed approximately 290 pounds, and the system had a fundamental bending frequency of about 15 cycles per second.

Wire strain gages were mounted on the panel spar near the root as sketched in figure 1 and were oriented so as to indicate panel deflections about two different axes. Strain gages were also attached to the cantilever beam (fig. 4) in the mount to indicate pitching motions of the model.

The strain-gage signals, the tunnel stagnation and static pressures, and the stagnation temperature were recorded by a recording oscillograph. The strain-gage traces on the oscillograph records were used to identify the start of flutter and to obtain the flutter frequency. In the present investigation the starts of flutter oscillations were very abrupt and definite on the oscillograph records. High-speed motion pictures were made during all runs and were used in observing the flutter mode. The models were tested at Mach numbers from 0.79 to 1.47 and at simulated altitudes from below sea level up to about 10,000 feet.

RESULTS AND DISCUSSION

The data obtained in the 21 runs of the investigation are summarized in table VI. The data from all the runs are plotted in figures 8 to 12 in the form of dynamic pressure as a function of Mach number. The margin-of-safety requirement was such that a satisfactory horizontal tail for the airplane would be flutter free at dynamic pressures up to 32 percent higher than those for sea-level altitude. Thus, if the models are assumed to represent the proposed airplane tail designs in all important respects, the models would demonstrate an adequate margin of safety for the airplane if they were flutter free at dynamic pressures up to 32 percent higher than those for simulated sea level. Curves indicating a simulated altitude of 5,000 feet, simulated sea-level altitude, and dynamic pressures 32 percent higher than simulated sea level are shown in figures 8 to 12.

Model CO-96 demonstrated an adequate flutter safety margin at Mach numbers up to 1.44 as is shown in figure 8. Flutter was obtained at a Mach number of 1.44 at a dynamic pressure above the flutter safety margin. The flutter mode, observed by means of the motion pictures taken during the runs, involved bending, torsion, and pitching motion of the panel. This was also shown by oscillograph records of the output of the strain gages on the cantilever beam in the mount. The onset of flutter was sudden and the oscillation amplitude diverged rapidly. The model failed after a few cycles. Although the start of flutter was definite, motion pictures and oscillograph records of the strain-gage signals indicated that the model exhibited pitching and yawing motions during all runs and before the start of flutter. These oscillations may be a function of the air turbulence and since the turbulence in the tunnel is different from that in the atmosphere, it is not known what significance the model oscillations have in regard to the airplane.

As shown in figure 9, models HO-95 and HO-99 had an adequate flutter safety margin at Mach numbers up to 1.14. At higher Mach numbers, however, these models displayed an inadequate safety margin. Flutter was obtained on model HO-99 at a Mach number of 1.14 and on model HO-95 at a Mach number of 1.42. The flutter mode and general behavior of these models were similar to those of model CO-96. It should be noted that, as mentioned previously, the chosen stiffness reduction due to aerodynamic heating which the high-temperature models were designed to simulate is probably more severe than would be encountered at the Mach numbers of the present investigation; thus, the model results may be conservative.

Inasmuch as the flutter mode observed for models CO-96, HO-95, and HO-99 included a significant amount of pitch deflection, in order to obtain a configuration for the high-temperature models of the original horizontal tail design which would be flutter free over the Mach number range of the tests, the effect of increased root pitching stiffness was
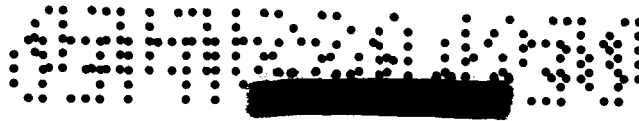
investigated. Models HO-137 and HO-118 had values of root pitching stiff-
ness of 137 percent and 118 percent of the scaled airplane value, respec-
tively, with about the same values of root yaw stiffness as the previous
models (table III). These models demonstrated an adequate flutter safety
margin at Mach numbers up to 1.47 (figs. 10 and 11), and no flutter was
encountered at dynamic pressures higher than the safety margin. It would
therefore appear that a moderate increase in the pitch stiffness (less
than 20 percent of the design value) would serve to eliminate the flutter
encountered for the high-temperature models of the original design at
Mach numbers near 1.4. The motion pictures taken during the tests of
models HO-137 and HO-118 (which did not flutter as shown in figs. 10
and 11) indicated that the pitching and yawing oscillations were of
lower amplitude than those noted before flutter in the tests of the pre-
vious configurations (figs. 8 and 9).

Model HR-101 had an adequate flutter safety margin at Mach numbers
up to 1.12 but had an inadequate safety margin at higher Mach numbers
(fig. 12). Flutter was encountered for this model at a Mach number
of 1.42, and the flutter mode and model behavior were the same as those
described previously for model CO-96. The similarity of flutter behavior
of this model to that of the models of the original design suggests that
an increase in the root pitching stiffness might also be beneficial for
the revised design.

CONCLUSIONS

A transonic flutter investigation has been made of dynamically and
elastically scaled models of the original design and of a revised design
for the all-movable horizontal tail of the X-15 airplane. The results
of the investigation supplied the following conclusions:

1. The standard-temperature model of the original design had an
adequate flutter safety margin (i.e., the model was flutter free at
dynamic pressures up to 32 percent higher than those for simulated sea-
level conditions) at Mach numbers up to 1.44.

2. Models which simulated the calculated effects of aerodynamic
heating for both designs had adequate flutter safety margins at Mach
numbers up to about 1.1 but had inadequate safety margins at higher
Mach numbers. However, the simulated design heating condition was
probably more severe than would be encountered at the Mach numbers of
the present investigation so that the model results may have been
conservative.
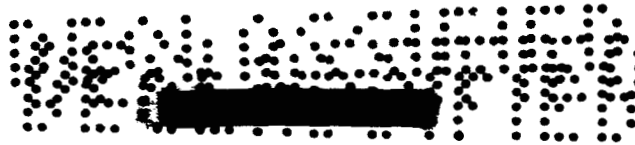
3. An increase in the pitching stiffness at the panel root for a high-temperature model of the original design to 118 percent of the scaled airplane design value produced a configuration which had an adequate flutter safety margin at Mach numbers up to about 1.46.

Langley Research Center,
National Aeronautics and Space Administration,
Langley Field, Va., October 20, 1960.
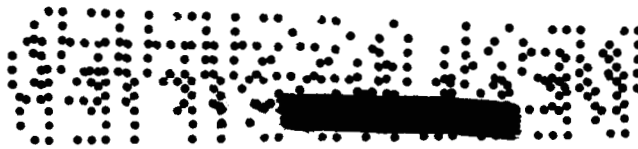
APPENDIX

MEASUREMENT OF FLEXIBILITY INFLUENCE COEFFICIENTS

A photograph of the system employed to measure the translational deflections of the panel is shown in figure 13. Twelve differential transformers were mounted above the model so that probes attached to their internal, sliding slugs rested on the influence coefficient stations. The readout device contains a differential transformer which can be connected to any one of the transformers above the model and which deflects an optical scale as it responds to changes in the magnetic flux in the transformer on the model induced by deflection of the model.

The output from a differential transformer is affected by the proximity of ferromagnetic material, so that it was necessary to calibrate each transformer while it was in the same environment as during the measurement. The transformers were therefore arranged in the locations they would have on the model (positions shown in fig. 7), and each transformer was deflected incrementally by means of a micrometer to obtain a factor to convert scale readings for that transformer into inches of deflection. Variations in the scale deflection readings for a range of known deflections of the micrometer were used to estimate the accuracy, linearity, and repeatability of the instrument readings. After calibration, the model was inserted and the undeflected scale reading for each of the transformers above the model was recorded. A load was applied to the model and the deflected scale readings of the transformers were recorded.

An optical system employing two theodolites was used to measure the angular deflections at the intersection of the pitch axis with the panel root. Two small mirrors were mounted at the intersection oriented normal to each other as in figure 7 so that pitching, yawing, and rolling angular deflections could be measured.

Loads were applied to the panel by means of a lever arm and strings and pulleys. The characteristics of the system were such that translational deflections for the yaw loading could not be read.

The translational and rotational deflection readings were converted into deflection (in feet or radians) per unit load to obtain the values in table IV(a). Note that the angular deflections measured for each unit load on the panel have the dimension radians per pound and that the translational deflections measured for the unit pitching and rolling moments have the dimension foot per foot-pound; these measurements are

labeled "semiangular influence coefficients." The matrix of angular influence coefficients has the dimensions radians per foot-pound. The pitch deflection for an applied pitching moment in table IV gives a value of pitching stiffness which agrees to within 0.4 percent with the value given in table III measured for the same model (HO-105) by means of the cathetometer system.

The calculated maximum error of the instrument used to measure the translational influence coefficients, obtained from the calibration data and checking of the weights used, varies according to the size of the deflection between $\pm 0.12 \times 10^{-5}$ ft/lb and $\pm 3.2 \times 10^{-5}$ ft/lb. The calculated maximum error of the semiangular influence coefficients measured with this instrument varies according to the size of the deflection between $\pm 0.11 \times 10^{-5}$ per pound and $\pm 3.2 \times 10^{-5}$ per pound. The best indication of the overall accuracy of the measurements is obtained from the symmetrization of the matrix of table IV(a) into the matrix of table IV(b). The symmetrical matrix in table IV(b) was obtained by averaging the corresponding off-diagonal elements of the original matrix. Of the off-diagonal elements measured, not including the angular or semiangular influence coefficients, 85 percent are within ± 3 percent of the averaged values, 95 percent are within ± 5 percent of the averaged values, and the remaining 5 percent are within ± 10 percent of the averaged values. The off-diagonal elements of the angular and semiangular influence coefficients are in somewhat poorer agreement.

REFERENCES

1. Lauten, William T., Jr., and Hess, Robert W.: Experimental and
   Calculated Supersonic Flutter Characteristics of Models of the
   X-15 Horizontal and Vertical Tails. NASA TM X-176, 1959.

2. Lauten, William T., Jr., Levey, Gilbert M., and Armstrong, William O.:
   Investigation of an All-Movable Control Surface at a Mach Number
   of 6.86 for Possible Flutter. NACA RM L58B27, 1958.

3. Landrum, L. L.: Estimated Aeroelastic Characteristics for the
   X-15 Airplane (NAA Model Designation NA-240). Rep. No. NA-59-471,
   North American Aviation, Inc., Apr. 16, 1959.

4. Anon.: Standard Atmosphere - Tables and Data for Altitudes to
   65,800 Feet. NACA Rep. 1235, 1955. (Supersedes NACA TN 3182.)

5. Land, Norman S., and Abbott, Frank T., Jr.: Method of Controlling
   Stiffness Properties of a Solid-Construction Model Wing. NACA
   TN 3423, 1955.

6. Unangst, John R., and Jones, George W., Jr.: Some Effects of Sweep
   and Aspect Ratio on the Transonic Flutter Characteristics of a
   Series of Thin Cantilever Wings Having a Taper Ratio of 0.6. NACA
   RM L55I13a, 1956.

7. Bursnall, William J.: Initial Flutter Tests in the Langley Transonic
   Blowdown Tunnel and Comparison With Free-Flight Flutter Results.
   NACA RM L52K14, 1953.

L
3
0
9

TABLE I.- GEOMETRIC PROPERTIES OF MODELS

Streamwise airfoil section . . . . Modified 66A005
Sweepback of quarter-chord line, deg 45
Panel span, ft 0.473
Streamwise panel root chord, ft 0.588
Panel area, sq ft 0.181
Panel aspect ratio 1.24
Panel taper ratio 0.30
Fuselage diameter, ft 0.250
Gap between panel root and fuselage, ft 0.007
Planform semispan, ft 0.605
Maximum streamwise chord based on extension of panel
    to fuselage center line, ft 0.703
Planform area based on extension of panel to fuselage
    center line, sq ft 0.532
Planform aspect ratio based on extension of panel to
    fuselage center line 2.752
Planform taper ratio based on extension of panel to
    fuselage center line 0.25

TABLE II.- DESIGN SCALE FACTORS OF PERTINENT MODEL AND FLOW QUANTITIES

$$\left[\frac{\rho_M}{\rho_A} = 1.275; \ \frac{T_M}{T_A} = 0.786\right]$$

Quantity	Design scale factor	
	Symbolical	Numerical
Fundamental quantities		
Length	l	1/12
Mass	$m = \left(\frac{\rho_M}{\rho_A}\right)l^3$	7.378×10^{-4}
Time	$t = \left(\frac{T_M}{T_A}\right)^{-1/2}l$	9.400×10^{-2}
Derived quantities		
Stream velocity	lt^{-1}	0.887
Stream dynamic pressure	$l^{-1}mt^{-2}$	1.002
Moment of inertia	l^2m	5.124×10^{-6}
k_θ, k_ϕ, k_ψ	l^2mt^{-2}	5.799×10^{-4}
EI and GJ	l^3mt^{-2}	0.483×10^{-4}
Flexibility influence coefficients: Translational	$m^{-1}t^2$	11.98
Semiangular	$l^{-1}m^{-1}t^2$	143.7
Angular	$l^{-2}m^{-1}t^2$	1,725
Natural vibration frequency	t^{-1}	10.64

L-309

TABLE III.- PHYSICAL PROPERTIES OF MODELS

Model designation	Natural vibration frequencies					Structural damping coefficient, g	Stiffness at intersection of pitch axis and panel root			Panel mass, m', slug	Moment of inertia about axes through panel center of gravity		
	First bending, cps	Yaw, cps	First torsion, cps	Second bending, cps	Second torsion, cps		k_ϕ, ft-lb/radian	k_θ, ft-lb/radian	k_ψ, ft-lb/radian		I_ϕ, slug-ft²	I_θ, slug-ft²	I_ψ, slug-ft²
CO-96	160	257	459	601	940	0.007	-------	0.413×10^3	1.074×10^3	0.536×10^{-2}	-------	-------	-------
HO-95	135	248	400	463	682	.018	-------	.409	.991	.513	-------	-------	-------
HO-99	140	268	427	476	700	.012	-------	.425	1.156	.492	-------	-------	-------
HO-105	124	272	385	476	693	-------	-------	.450	-------	.494	1.166×10^{-4}	1.015×10^{-4}	2.014×10^{-4}
HO-137	128	264	404	502	695	.015	-------	.590	1.040	.494	1.166	1.015	2.014
HO-118	126	263	402	493	683	.011	-------	.508	1.139	.494	1.166	1.015	2.014
HR-101	147	290	380	476	606	.010	1.470×10^3	.433	1.657	.659	1.422	1.354	2.680

TABLE IV.- FLEXIBILITY INFLUENCE COEFFICIENTS FOR MODEL HO-105

[Stations shown in fig. 8]
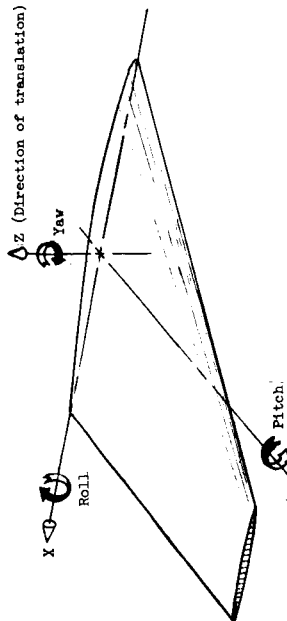
Coordinate system used. Arrows indicate positive directions.

Z (Direction of translation)
Yaw
Roll
Pitch
X
Y'

(a) Measured influence coefficients

| Influence-coefficient station	Influence coefficients for vertical load at station -												Influence coefficients for twist load at root -		
	1	2	3	4	5	6	7	8	9	10	11	12	Pitch	Roll	Yaw
	Translational, ft/lb												Semiangular, ft/ft-lb		
1	7.68×10^{-5}	-1.2×10^{-5}	5.50×10^{-5}	-2.0×10^{-5}	3.02×10^{-5}	-3.14×10^{-5}	1.2×10^{-5}	-3.94×10^{-5}	-0.92×10^{-5}	-4.62×10^{-5}	-3.2×10^{-5}	-5.2×10^{-5}	35.4×10^{-5}	12.9×10^{-5}	----
2	-1.3	3.22	.85	4.72	3.06	6.44	5.25	9.00	8.12	10.5	10.8	12.5	-20.9	13.1	----
3	5.36	.85	1.8	2.2	8.92	4.08	9.08	5.55	9.83	6.75	10.5	8.50	13.8	21.2	----
4	-2.2	4.62	9.17	12.2	7.59	17.8	14.7	23.3	22.7	28.7	30.7	34.0	-35.5	21.5	----
5	3.02	3.00	3.81	7.58	17.3	13.8	21.5	19.8	26.7	25.8	33.0	32.2	-5.42	32.6	----
6	-3.00	6.39	8.92	17.8	13.7	33.41	27.7	45.95	45.50	58.9	64.0	73.8	-50.1	32.6	----
7	1.2	5.50	5.25	14.6	21.2	28.14	39.24	41.72	54.17	56.38	70.1	72.7	-23.2	38.1	----
8	-3.94	8.12	9.42	23.0	19.2	45.87	41.62	70.52	71.77	96.00	107.9	122.9	-61.9	39.0	----
9	-.78	7.68	6.31	22.5	26.3	45.70	54.62	72.37	93.67	106.7	133.2	142.2	-45.3	47.3	----
10	-4.94	9.83	10.3	28.62	25.2	59.39	56.87	96.17	105.6	143.9	166.9	195.1	-73.8	46.4	----
11	-3.19	10.8	8.33	31.48	33.06	64.63	70.82	108.1	133.1	167.7	214.0	236.9	-66.5	56.0	----
12	-5.62	11.5		34.60	31.72	73.79	72.65	124.1	141.1	196.8	237.5	283.4	-87.3	54.3	----
Rotation at root -	Semiangular, radians/lb												Angular, radians/ft-lb		
Pitch	27.9×10^{-5}	-21.4×10^{-5}	13.8×10^{-5}	-32.4×10^{-5}	-6.1×10^{-5}	-41.3×10^{-5}	-22.7×10^{-5}	-51.0×10^{-5}	-49.2×10^{-5}	-60.7×10^{-5}	-66.7×10^{-6}	-85.0×10^{-5}	223×10^{-5}	-2.8×10^{-5}	-14.7×10^{-5}
Roll	16.0	10.7	22.4	18.1	29.8	25.6	40.0	34.6	44.8	45.2	55.2	52.3	-.5	108	-9.2
Yaw	3.7	-4.6	0	-4.8	-3.2	-6.4	-8.5	-12.8	-13.6	-14.4	-19.2	-14.4	-17.4	-22.0	77.6

TABLE IV.- FLEXIBILITY INFLUENCE COEFFICIENTS FOR MODEL HO-105 - Concluded

[Stations shown in fig. 8]

(b) Symmetrical matrix of influence coefficients

Influence-coefficient station	Influence coefficients at station -												Influence coefficient at root -		
	1	2	3	4	5	6	7	8	9	10	11	12	Pitch	Roll	Yaw
	Translational, ft/lb												Semiangular, per lb		
1	7.68x10⁻⁵	-1.2x10⁻⁵	5.43x10⁻⁵	-2.1x10⁻⁵	3.02x10⁻⁵	-3.07x10⁻⁵	1.2x10⁻⁵	-3.94x10⁻⁵	-0.85x10⁻⁵	-4.78x10⁻⁵	-3.2x10⁻⁵	-5.4x10⁻⁵	31.6x10⁻⁵	14.4x10⁻⁵	3.7x10⁻⁵
2		3.22	.85	4.67	3.03	6.42	5.58	8.56	7.90	10.2	10.8	12.0	-21.2	11.9	-4.6
3			9.33	2.0	9.05	3.94	9.00	5.40	9.62	6.53	10.4	8.42	13.8	21.8	0
4				12.2	7.58	17.8	14.6	23.2	22.6	28.7	31.1	34.3	-34.0	19.8	-4.8
5					17.3	13.8	21.4	19.5	26.5	25.5	33.0	32.0	-5.8	31.2	-3.2
6						33.41	27.9	45.91	45.60	59.1	64.3	73.8	-45.7	29.1	-6.4
7							39.24	41.67	54.40	56.62	70.5	72.7	-23.0	39.0	-8.5
8								70.52	72.07	96.08	108.0	123.5	-56.4	36.8	-12.8
9									95.67	106.2	133.2	141.6	-47.2	46.0	-13.6
10										143.9	167.3	196.0	-67.2	44.8	-14.4
11											214.0	237.2	-66.6	55.6	-19.2
12												283.4	-86.2	53.3	-14.4
Rotation at root -													Angular, radians/ft-lb		
Pitch													225x10⁻⁵	-1.6x10⁻⁵	-16.0x10⁻⁵
Roll														108	-15.6
Yaw															77.6

TABLE V.- STRIP PROPERTIES OF MODELS WHICH SIMULATED ORIGINAL AND REVISED DESIGNS
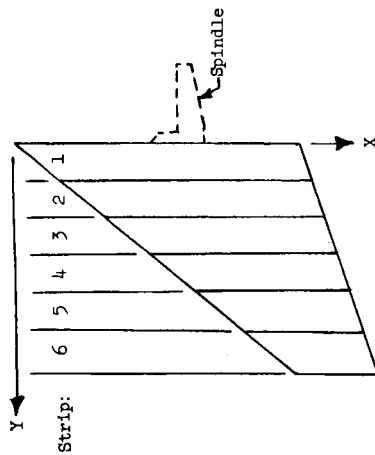
(a) Repaired model HO-99; streamwise strips

Strip	Mass of strip, m_s, slugs	Streamwise center-of-gravity location of strip, measured from leading edge, x_{cg}, percent chord	Mass moment of inertia in pitch about lateral axis through strip center of gravity, I_s, slug-ft²	Strip width, δ_s, ft	Average streamwise strip semichord, b_s, ft	Spanwise position of strip center of gravity, y_{cg}, percent span
1	1.564×10^{-3}	49.8	2.182×10^{-5}	0.076	0.278	5.5
2	.8116	52.2	1.009	.076	.245	24.1
3	.6157	48.7	.616	.076	.212	40.1
4	.5437	44.3	.501	.076	.179	56.4
5	.4029	47.1	.234	.085	.144	73.5
6	.3036	42.8	.103	.085	.106	91.3
Spindle	.6852	[a]67.1	-------	----	-----	-10.4
Total mass:	4.9267					

[a] x_{cg} of spindle is measured from extended leading edge and is given in percent of extended chord.

TABLE V.- STRIP PROPERTIES OF MODELS WHICH SIMULATED ORIGINAL AND REVISED DESIGNS - Concluded

Strip: 6 5 4 3 2 1

56.78-percent-chord line
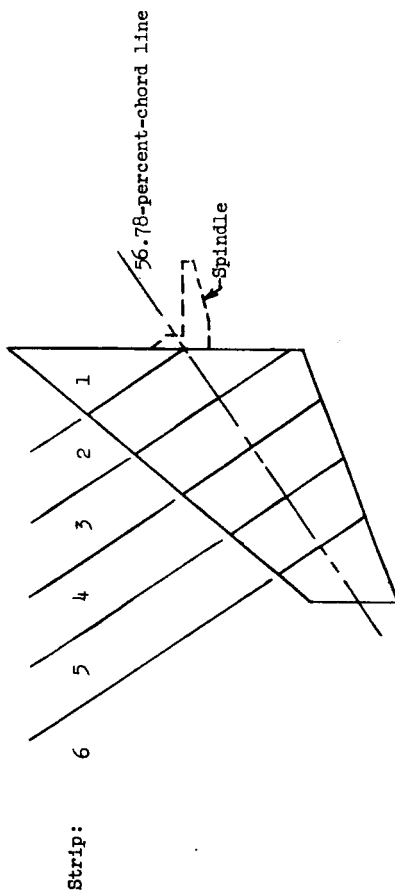
Spindle

(b) Model similar to model HR-101; properties of strip 1 and spindle were measured on model HR-101; strips cut normal to 56.78-percent-chord line

Strip	Mass of strip, slug	Distance of strip center of gravity from 56.78 percent chord measured normal to 56.78-percent-chord line, positive rearward, ft	Moment of inertia of strip about 56.78-percent-chord line, slug-ft^2	Strip width along 56.78-percent-chord line, ft
1	0.00116	-0.14	26.4×10^{-6}	0
2	.00108	-.017	6.21	.112
3	.00089	-.078	8.12	.112
4	.00072	-.011	5.94	.112
5	.00056	-.011	2.93	.112
6	.00044	-.001	1.27	.134
Spindle	.00117	-----	--------	-----
Total mass:	0.00602			

TABLE VI.- COMPILATION OF TEST RESULTS

Model	k_θ, ft-lb/radian	Run	Model behavior (a)	f_f, cps	M	q, lb/sq ft	V, ft/sec	ρ, slugs/cu ft	T, °R	μ	$\dfrac{b_\alpha \omega_f}{V}$
CO-96	413	1	Q	---	0.806	1,731	823	0.0051	434	17.6	---
		2	Q	---	.948	2,163	975	.0045	440	20.0	---
		3	Q	---	1.149	2,920	1,155	.0044	420	20.4	---
		4	F	254	1.435	4,290	1,369	.0046	379	19.5	0.223
HO-95	409	5	Q	---	.835	2,029	869	.0054	451	15.9	---
		6	Q	---	.995	2,406	1,009	.0047	428	18.3	---
		7	Q	---	1.088	2,575	1,083	.0044	413	19.6	---
		8	F	220	1.419	3,216	1,328	.0036	364	23.9	.199
HO-99	425	9	F	229	1.138	2,681	1,114	.0043	399	19.2	.247
HO-137	590	10	Q	---	.803	1,793	845	.0050	461	16.6	---
		11	Q	---	.978	2,370	1,003	.0047	438	17.6	---
		12	Q	---	1.126	2,919	1,114	.0047	407	17.6	---
		13	Q	---	1.467	4,470	1,321	.0051	338	16.2	---
HO-118	508	14	Q	---	.805	1,758	850	.0049	464	16.9	---
		15	Q	---	.973	2,308	1,002	.0046	441	18.0	---
		16	Q	---	1.120	2,879	1,111	.0047	410	17.6	---
		17	Q	---	1.459	4,261	1,313	.0049	337	16.9	---
HR-101	433	18	Q	---	.788	1,449	809	.0044	438	25.1	---
		19	Q	---	.956	2,079	950	.0046	411	24.0	---
		20	Q	---	1.122	2,886	1,084	.0049	389	22.6	---
		21	F	260	1.423	3,492	1,315	.0040	356	27.6	.238

[a] Model behavior code: F, start of flutter; Q, maximum q, no flutter.
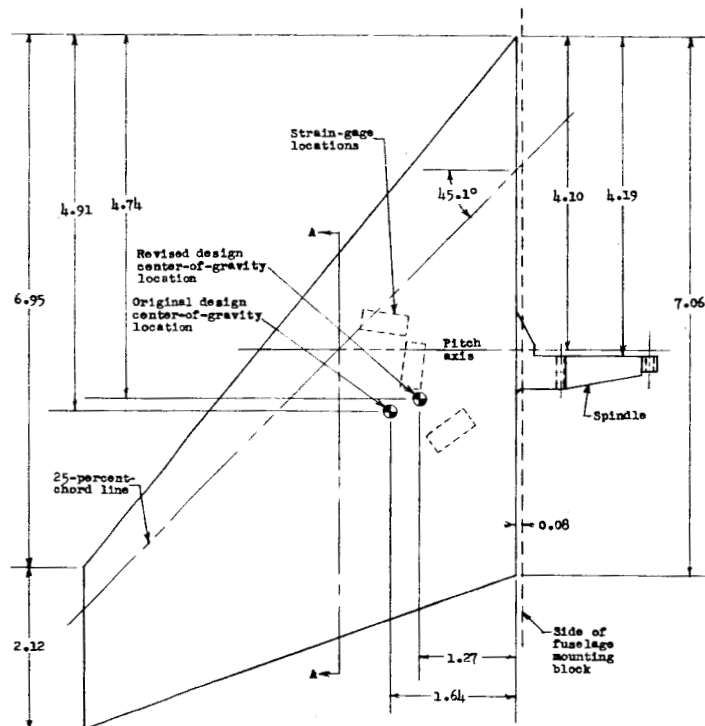
L-309

FRONT VIEW OF SPINDLE ON REVISED DESIGN

0.48

5.68   1.85

1.73

0.59

0.11   0.32

0.35   0.25
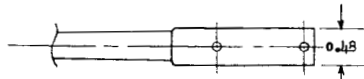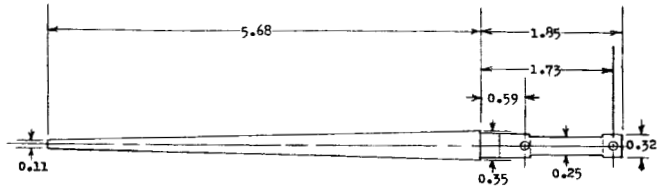
FRONT VIEW OF ORIGINAL DESIGN

MODIFIED 66A005

AIRFOIL ORDINATES PERCENT CHORD		
STATION	ROOT ORDINATE	TIP ORDINATE
L.E.	0.00	0.00
.10	.27	.35
.25	.41	.54
.50	.53	.73
.75	.58	.85
1.25	.65	.97
2.50	.79	1.05
5.00	1.04	1.20
7.50	1.27	1.35
10.00	1.46	1.50
15.00	1.77	1.77
20.00	2.00	2.00
25.00	2.18	2.18
30.00	2.32	2.32
35.00	2.42	2.42
40.00	2.48	2.48
45.00	2.50	2.50
50.00	2.49	2.49
55.00	2.44	2.44
60.00	2.35	2.35
65.00	2.18	2.18
67.00	2.09	2.08
T.E.	.50	.50

SECTION A-A

Strain-gage locations

45.1°

4.10   4.19

4.91   4.74

Revised design center-of-gravity location

Original design center-of-gravity location

Pitch axis

6.95

7.06

Spindle

25-percent-chord line

0.08

2.12

Side of fuselage mounting block

1.27

1.64

PLAN VIEW OF ORIGINAL AND REVISED DESIGNS

Center-of-gravity positions shown are for the panel including the spindle

Figure 1.- Sketch of panel. All dimensions are in inches.
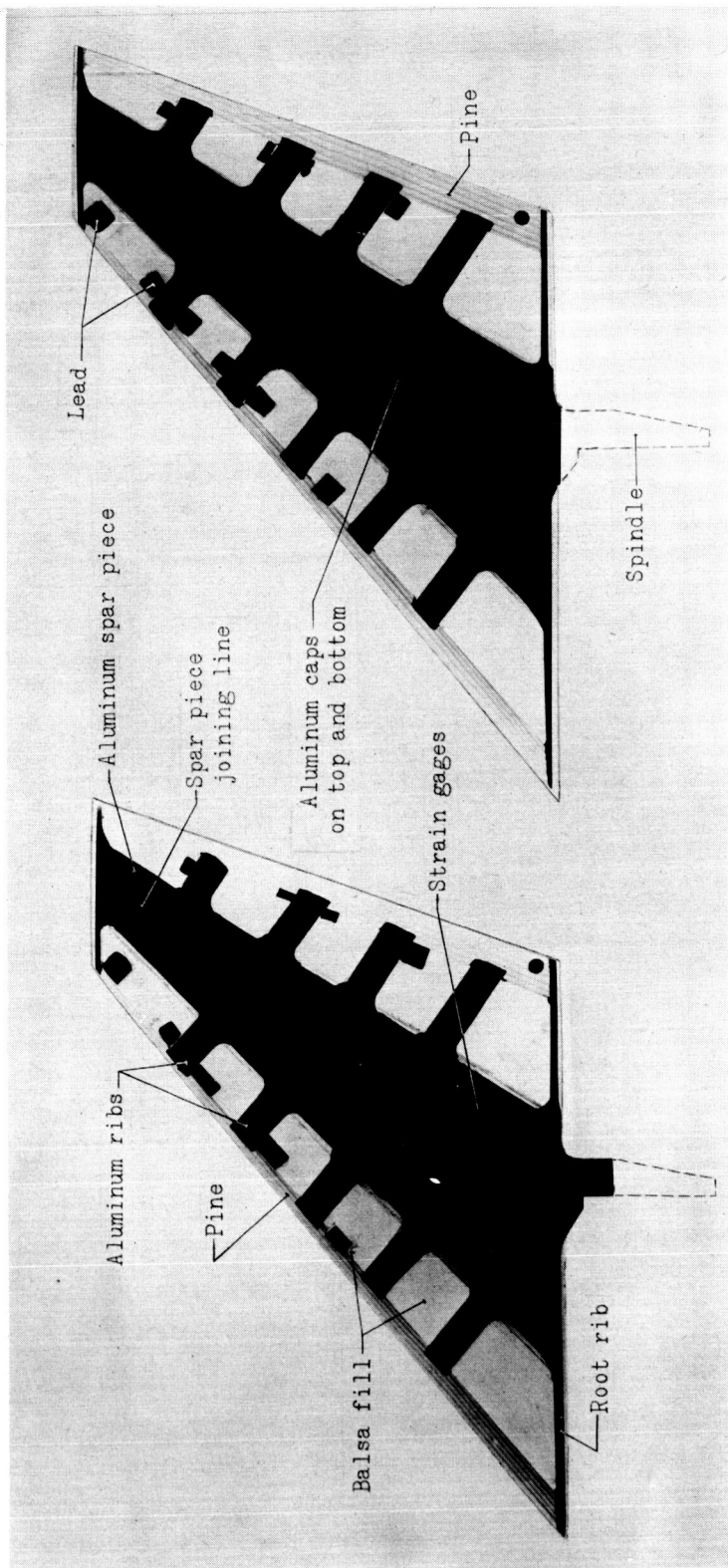
Figure 2.- X-ray photographs of models.   L-60-6912
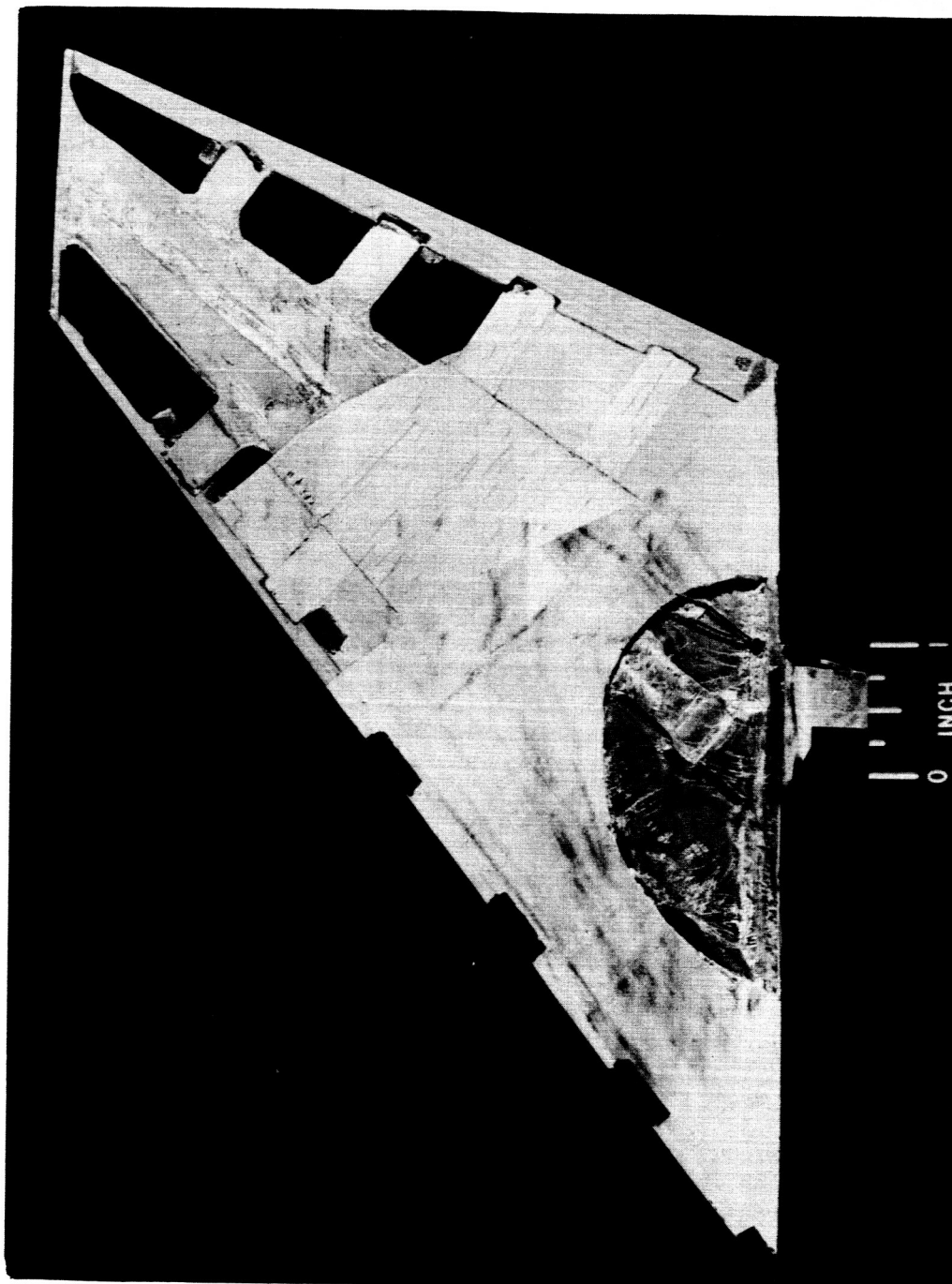
L-309

L-60-6913

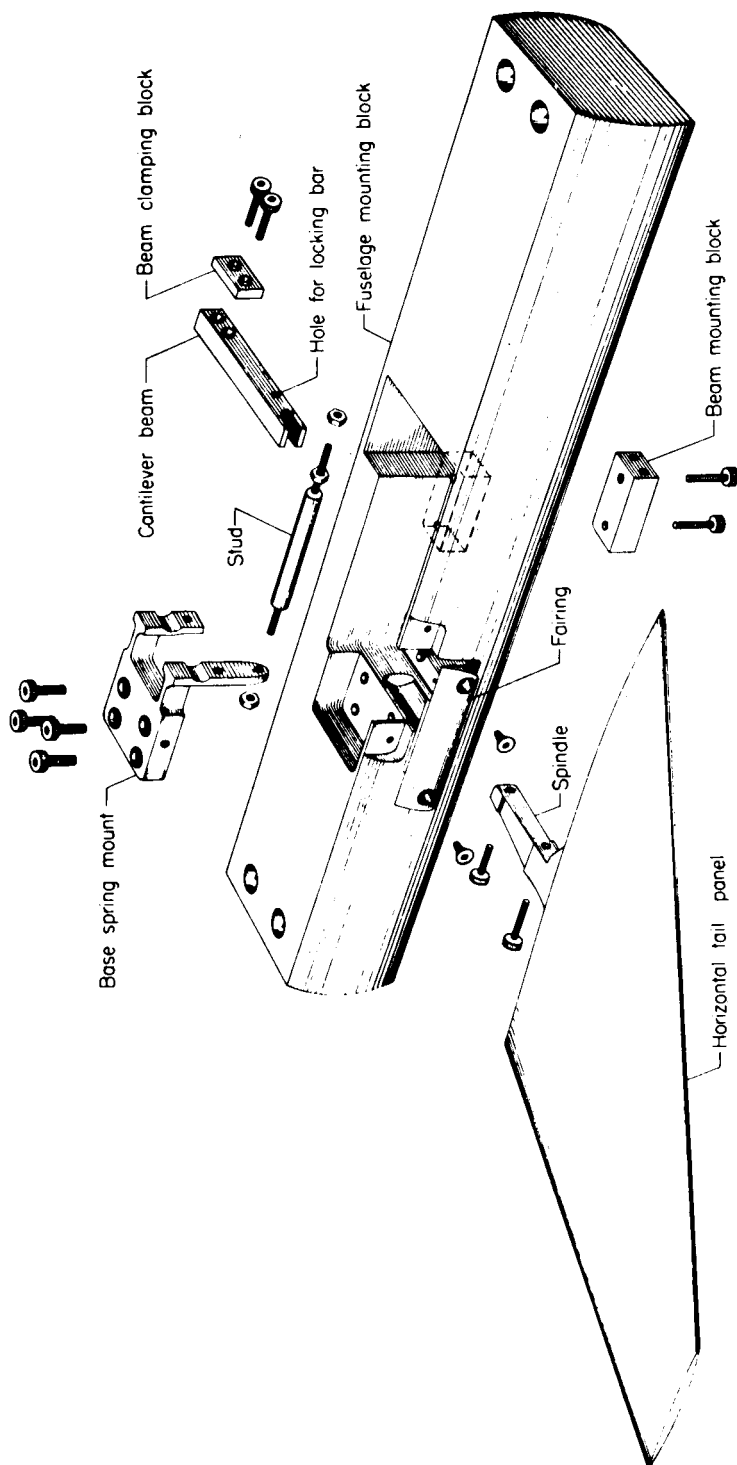Figure 3.- Photograph of a panel which has been cut away to expose internal structure.
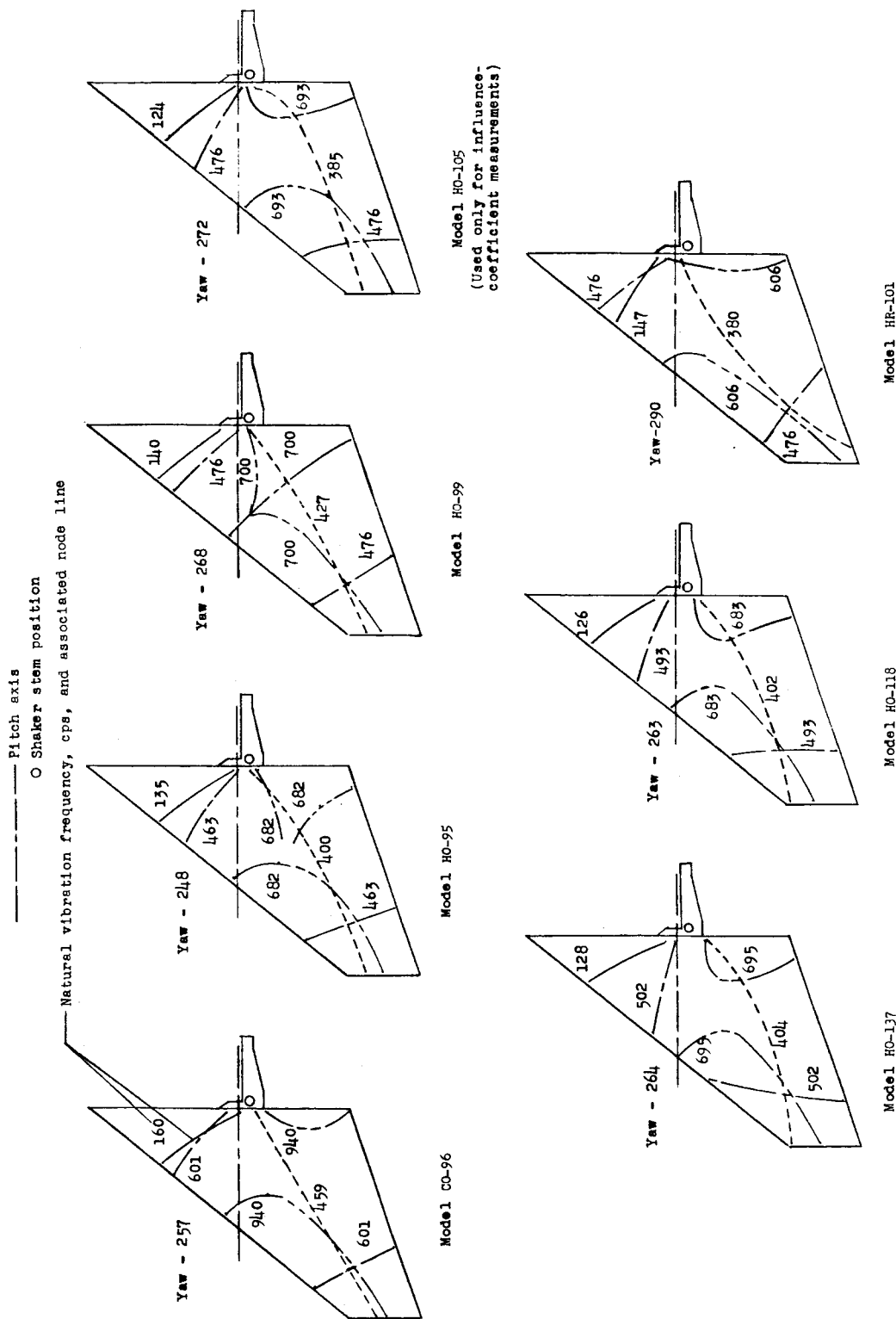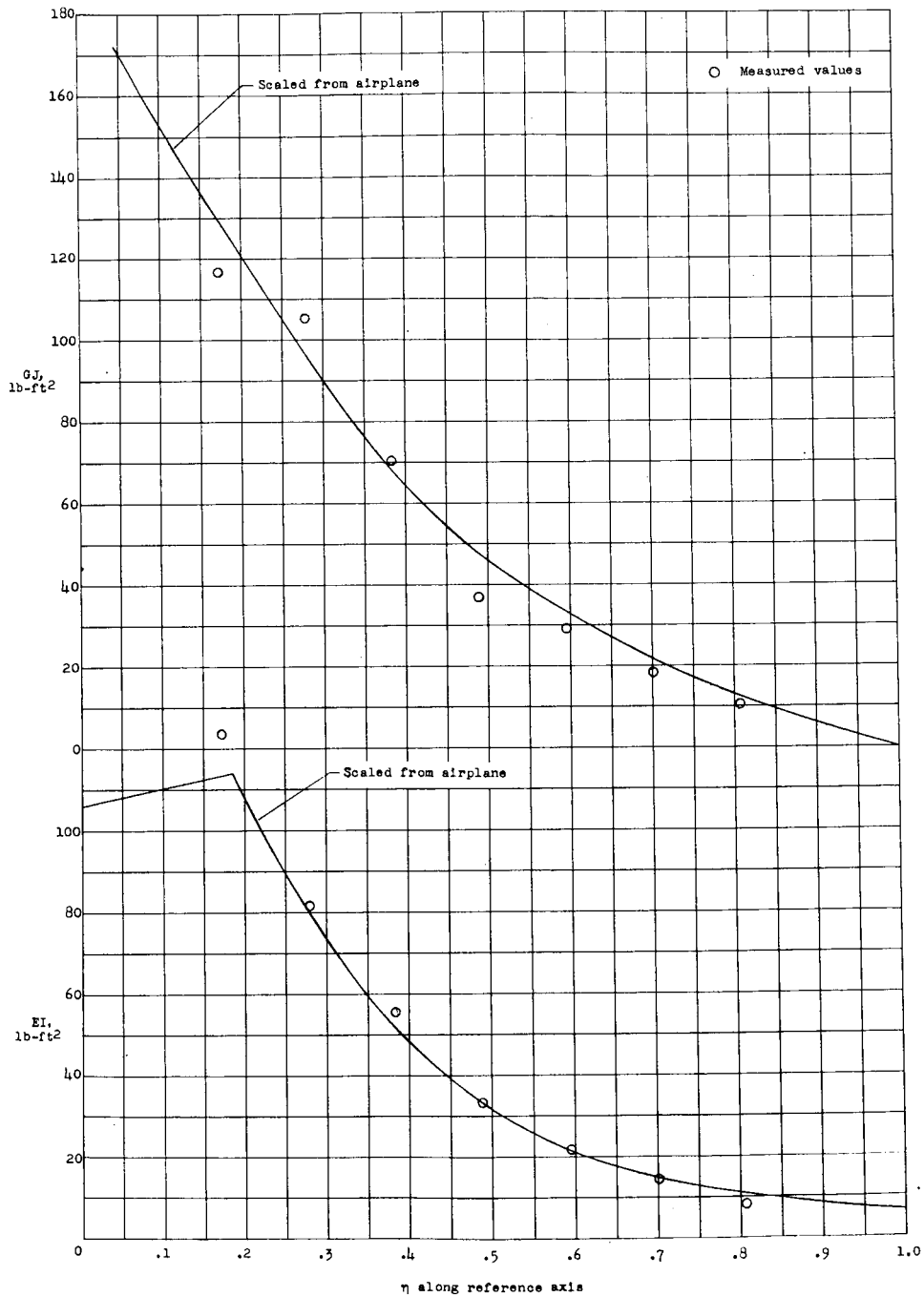
Figure 4.- Exploded drawing of model and mount.

L-309

Pitch axis
O Shaker stem position
Natural vibration frequency, cps, and associated node line

Yaw – 272

124

476

693

693

385

476

Model HO-105
(Used only for influence-
coefficient measurements)

Yaw – 268

140

476

700

700

427

476

Model HO-99

Yaw – 248

135

463

682

682

400

463

Model HO-95

Yaw – 257

160

601

940

940

459

601

Model CO-96

476

147

606

380

606

476

Yaw–290

Model HR-101

126

493

683

683

402

493

Yaw – 263

Model HO-118

128

502

695

695

404

502

Yaw – 264

Model HO-137

Figure 5.- Measured natural vibration frequencies and node lines for models as tested.

(a) Model CO-96.

Figure 6.- Measured panel bending and torsion stiffness distributions compared with scaled airplane stiffness distributions.
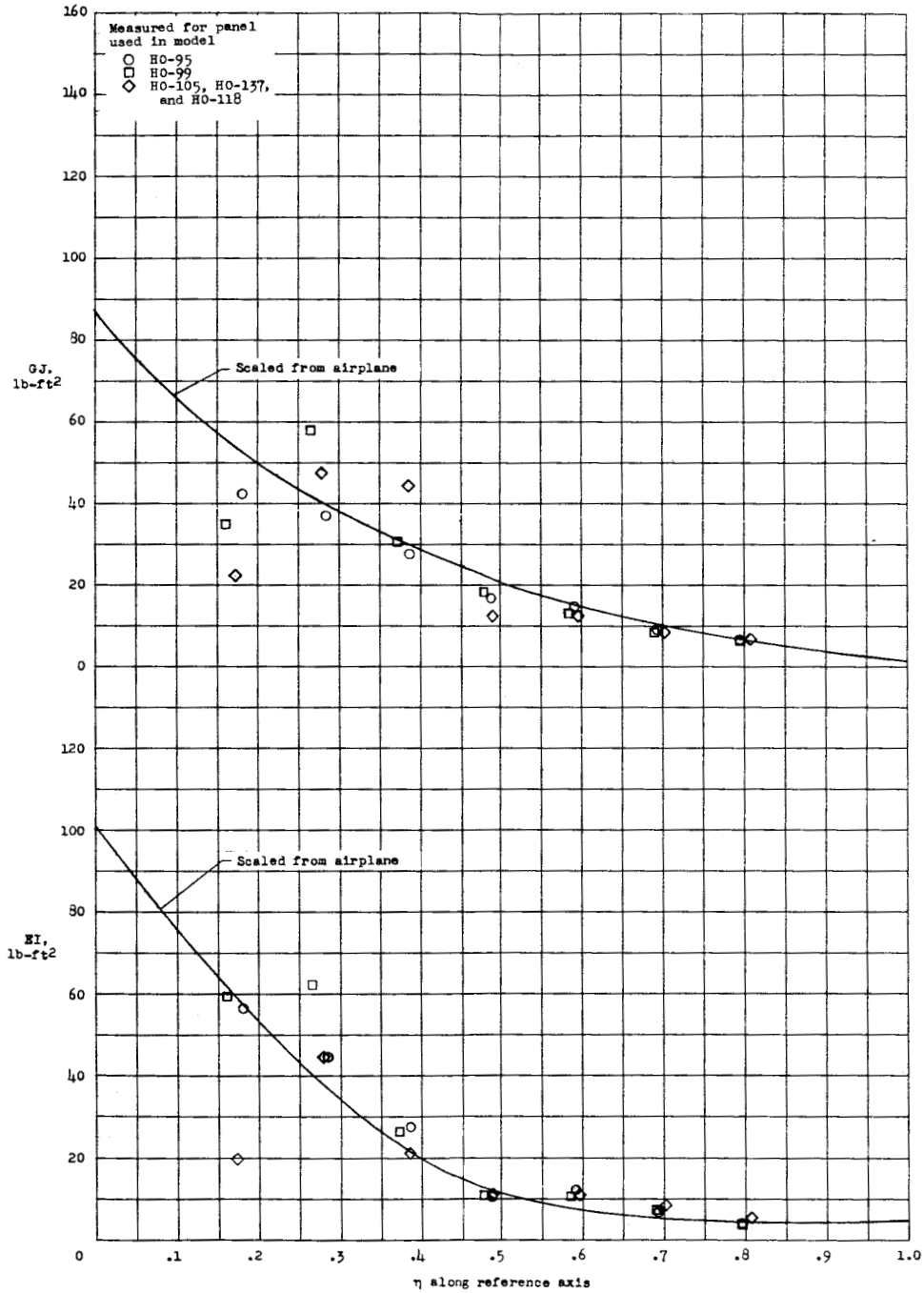
(b) Models of original design which simulated effects of aerodynamic heating.

Figure 6.- Continued.
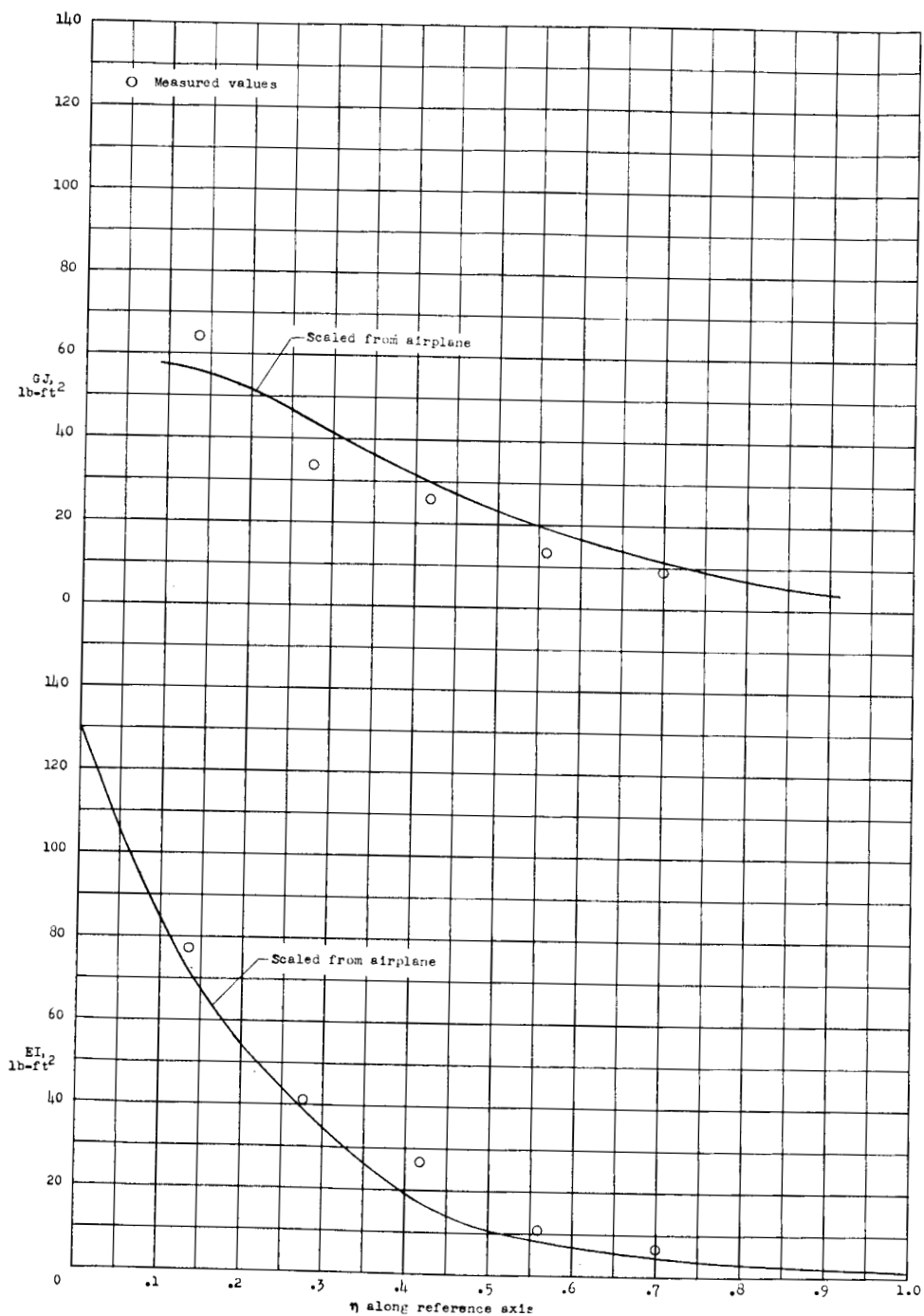
(c) Model HR-101.

Figure 6.- Concluded.
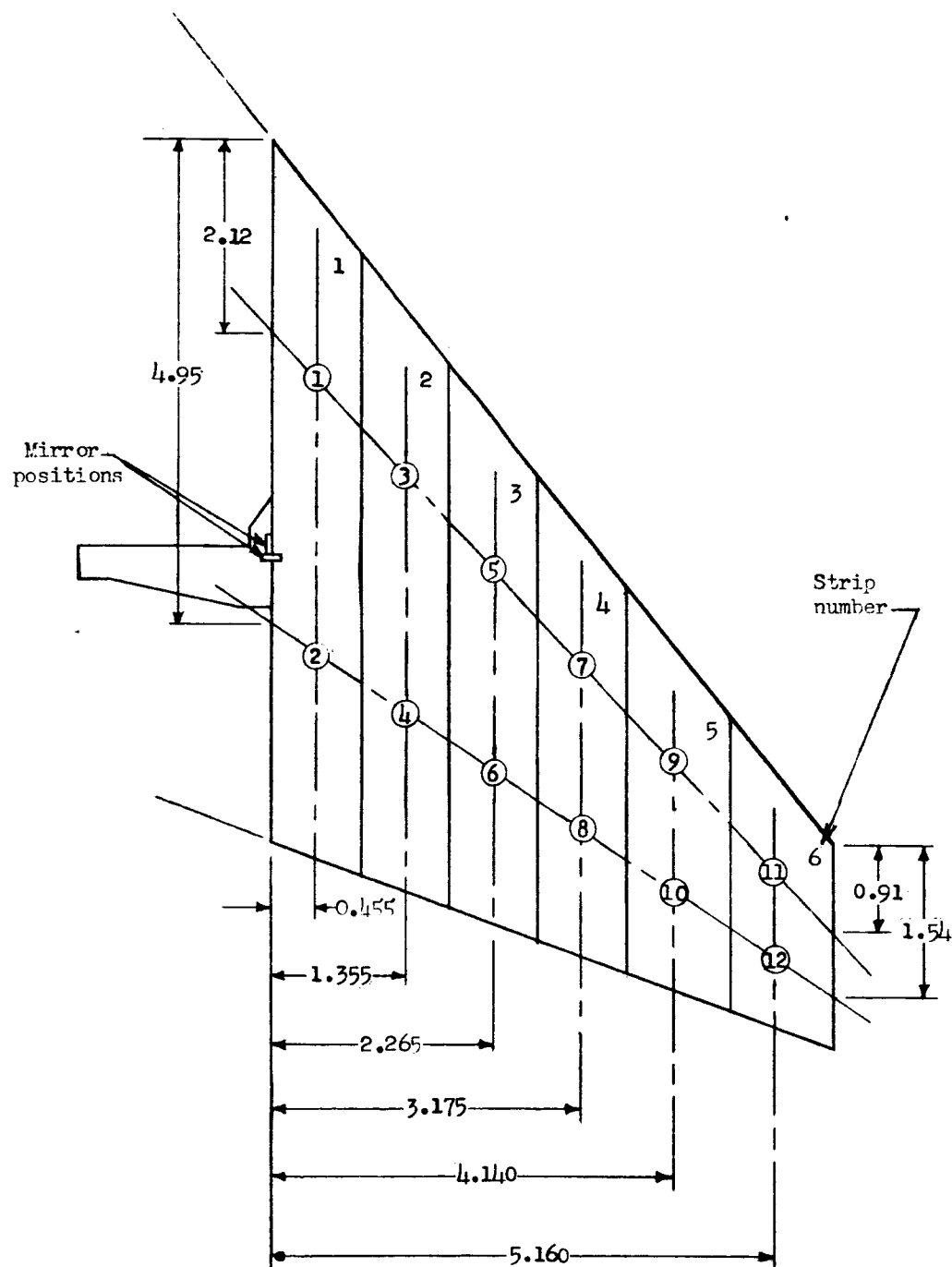
Figure 7.- Sketch of panel showing streamwise strips and influence coefficient stations. All dimensions are in inches. Circled numbers indicate stations at which influence coefficients were measured.
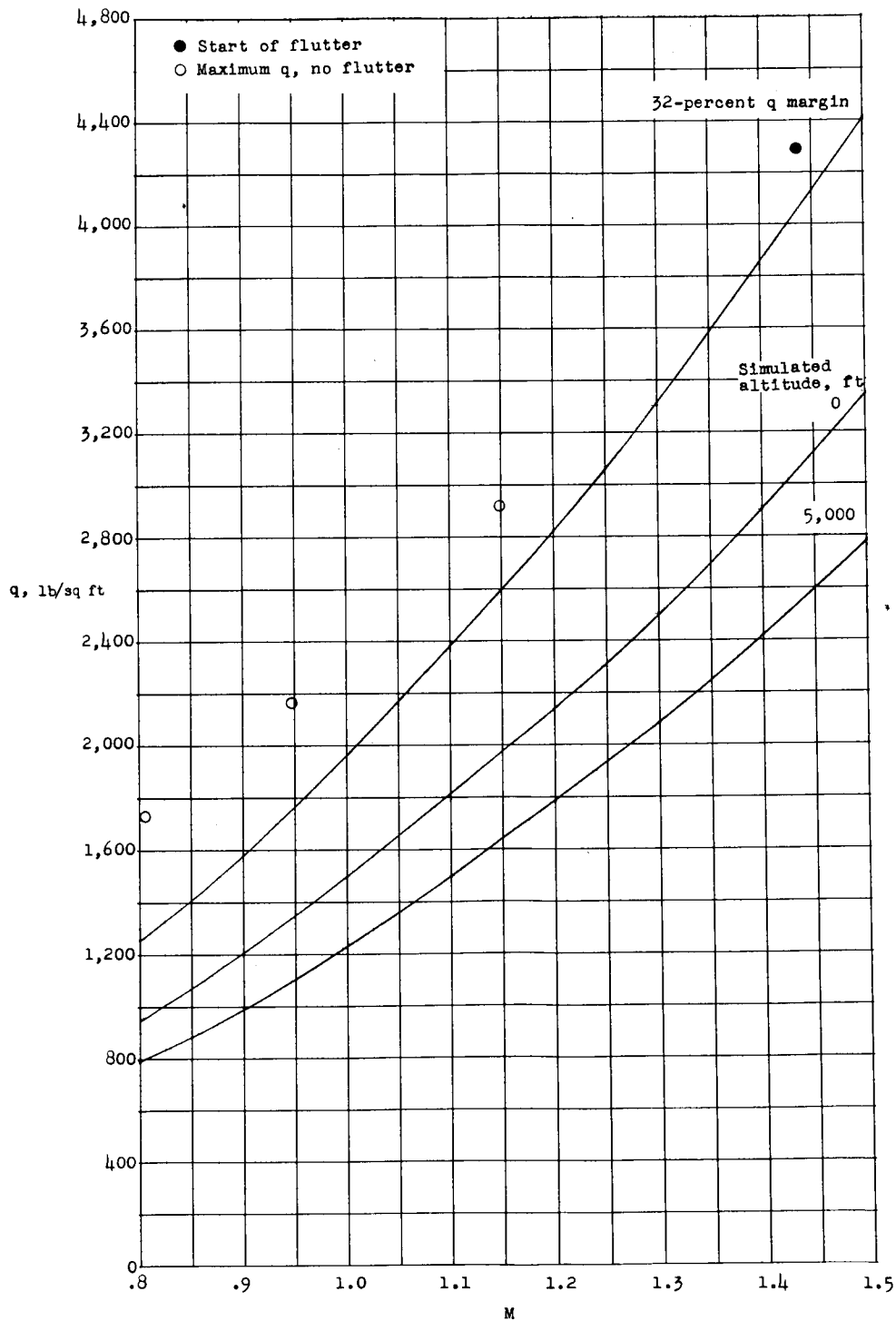
Figure 8.- Flutter characteristics of model CO-96.

L-309
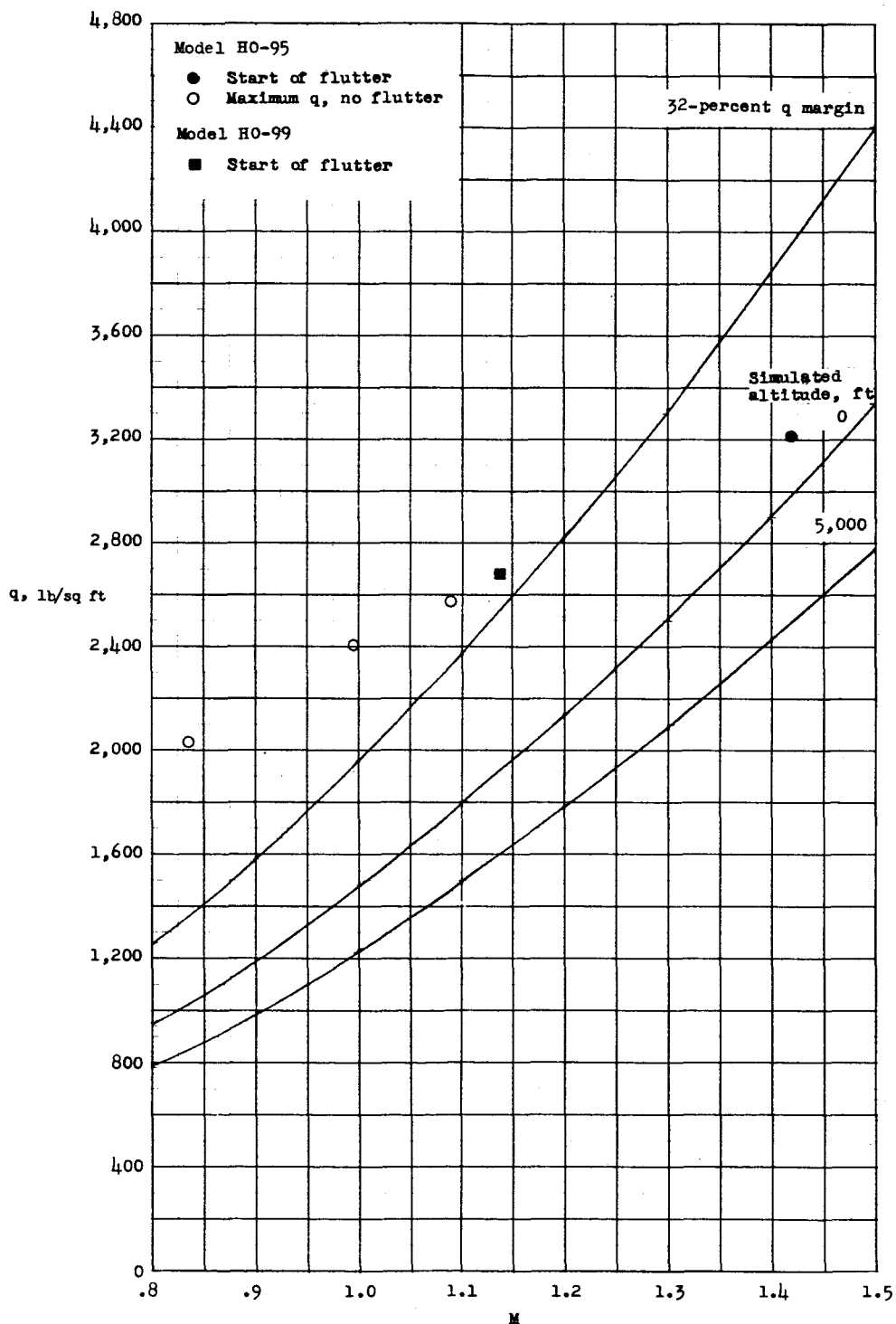
Figure 9.- Flutter characteristics of models HO-95 and HO-99.
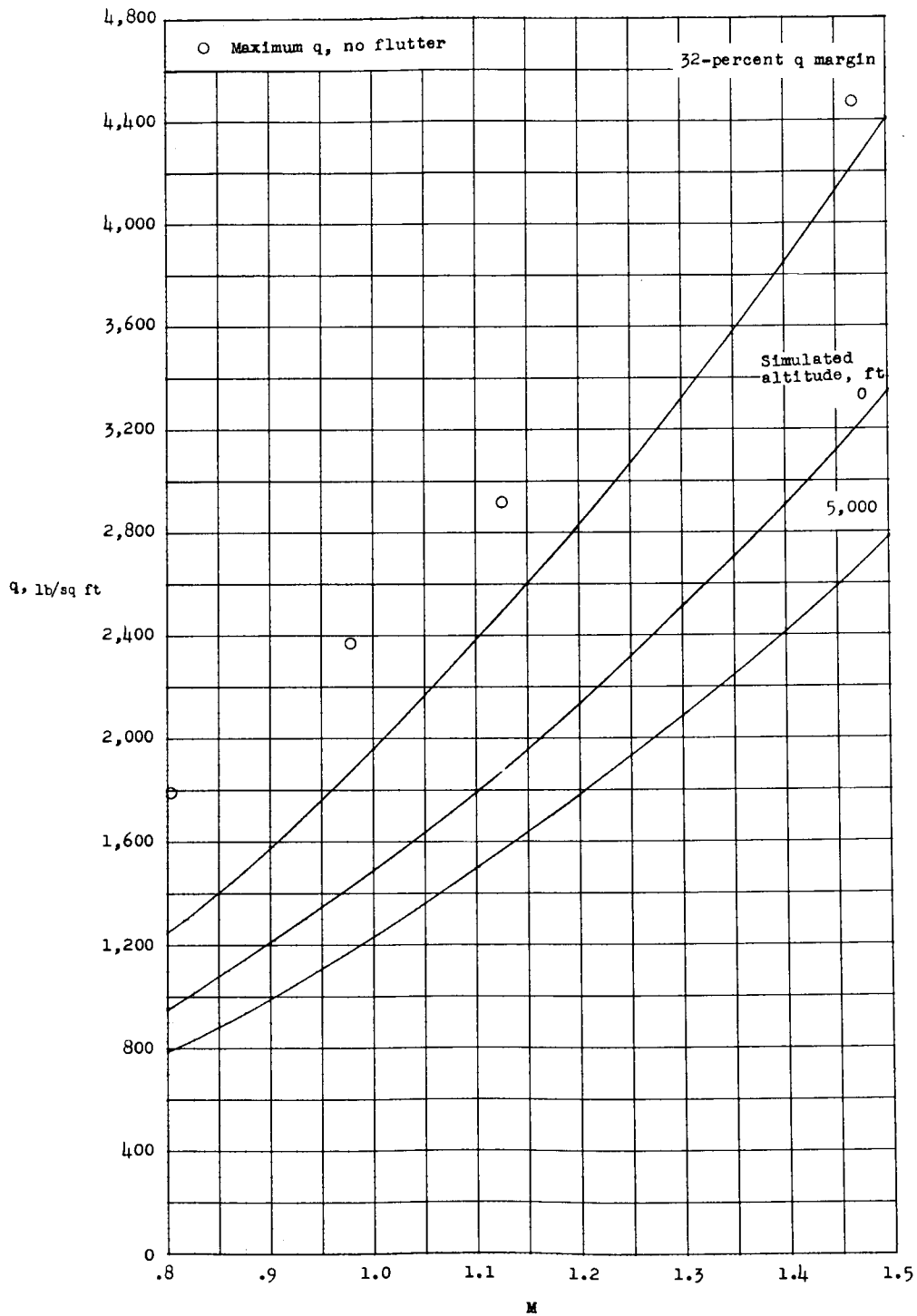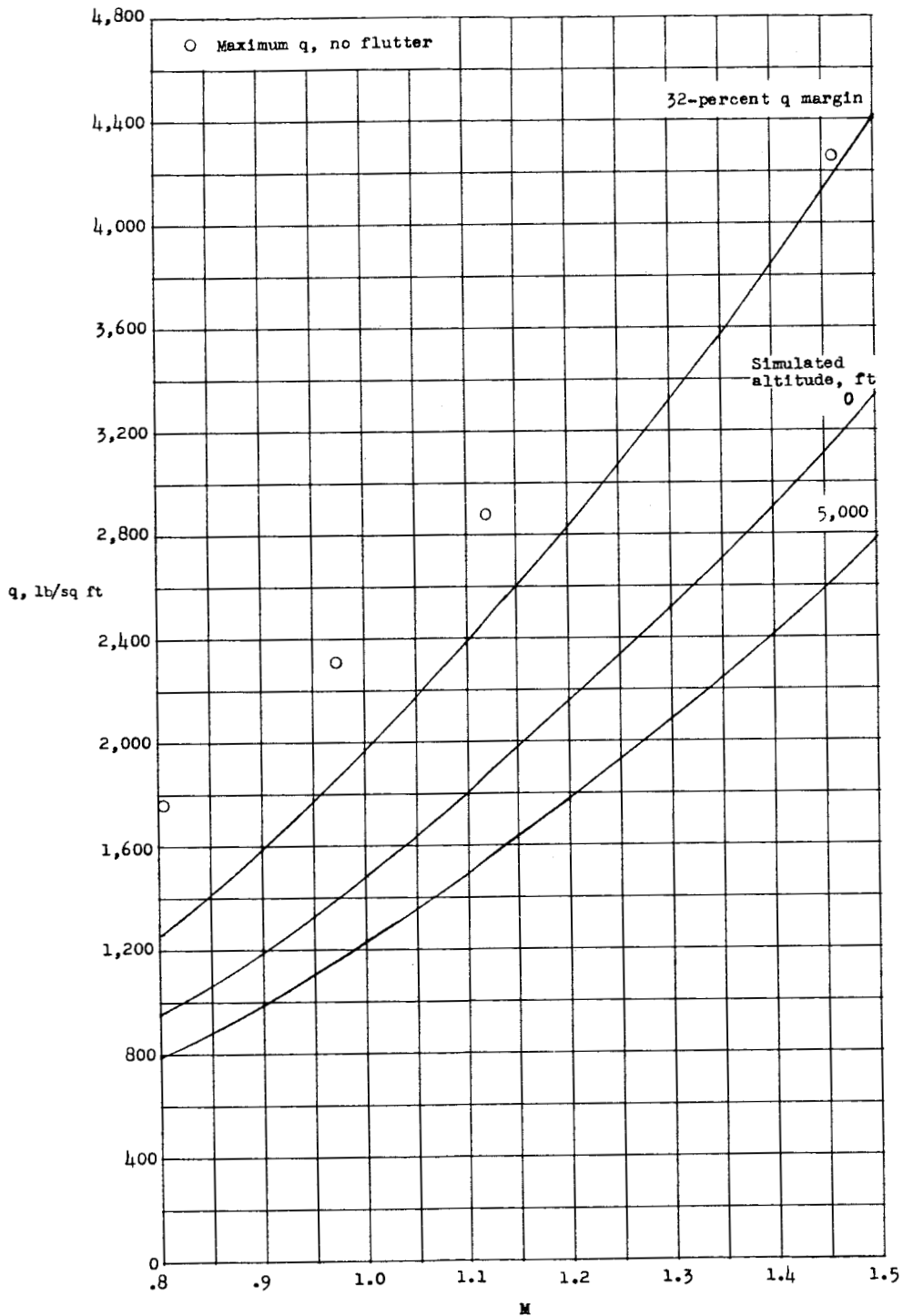
Figure 10.- Flutter characteristics of model HO-137.

Figure 11.- Flutter characteristics of model HO-118.
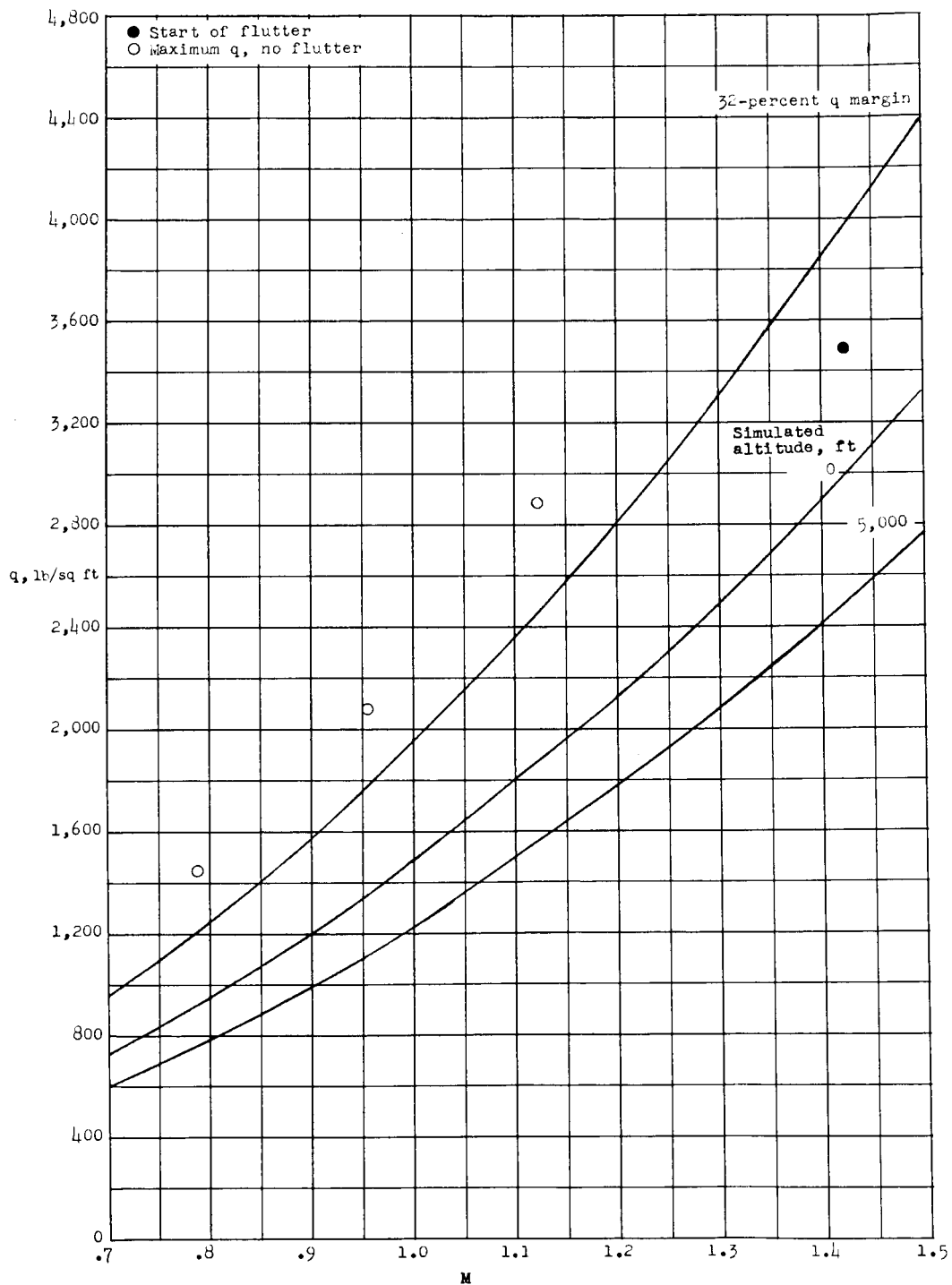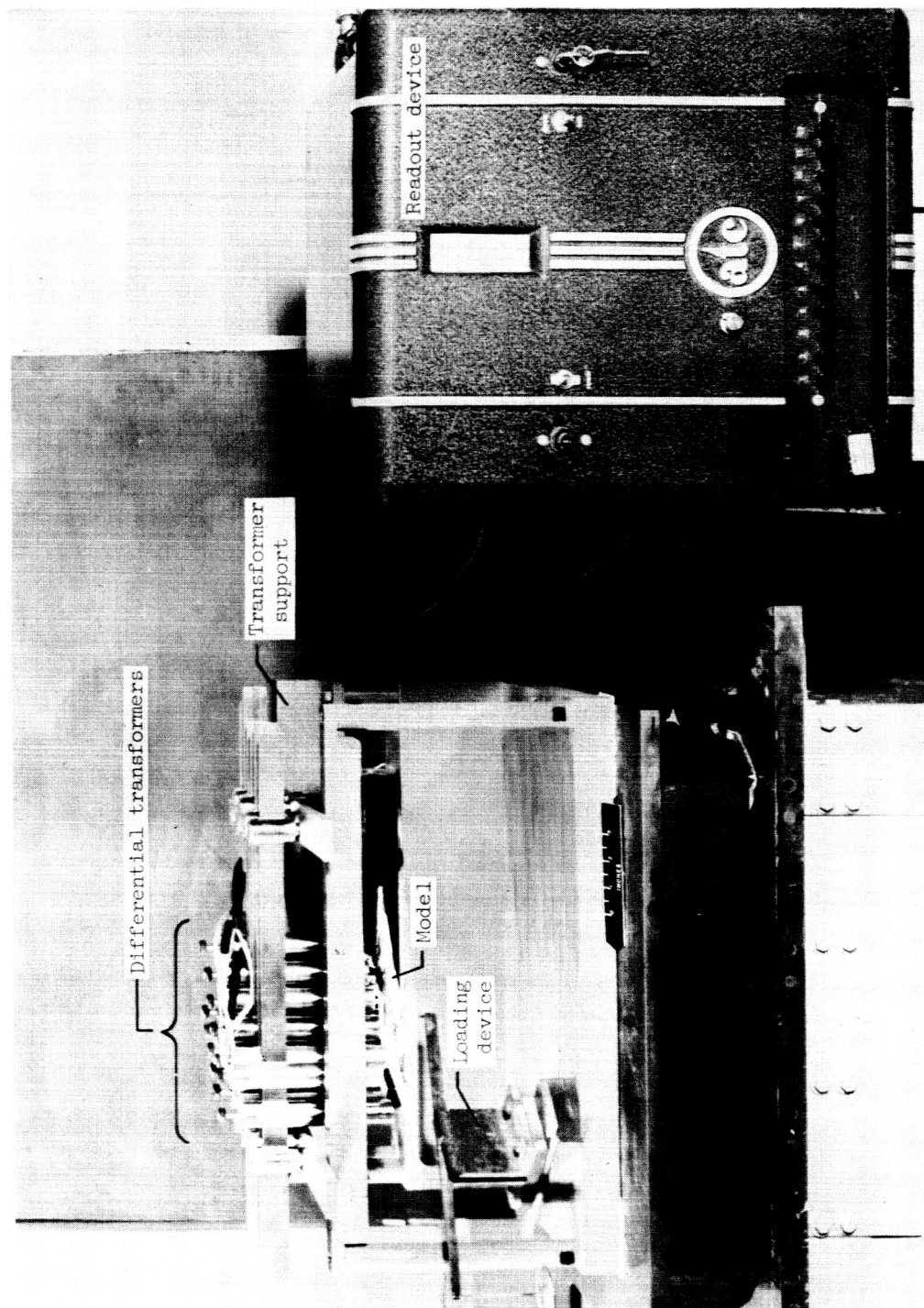
Figure 12.- Flutter characteristics of model HR-101.

DECLASSIFIED

Figure 13.- Equipment used to measure translational flexibility influence coefficients.

L-57-3220.1

L-309